

Cite this: *J. Mater. Chem. A*, 2024, **12**, 2070

# *In situ* wrapping carbon dots towards robust, durable and transparent tri-layer films with precise spectral conversion and excellent self-cleaning properties†

Sainan Zhang and Junhui He \*

To boost agricultural productivity and pave an eco-friendly way to solve the global food crisis, light conversion agents with spectrum matching, and high stability are promising candidates. Carbon dots (CDs) are regarded as viable nanomaterials for light conversion based on their unique physical and optical properties, particularly those that can mitigate aggregation-caused quenching (ACQ). Here, a series of polymer wrapped CDs, that overcome the ACQ and emit intense red-light in solid-state, were synthesized. Notably, the quantum yields of these solid-state CD-polymers are improved to 20.91%. Then a light conversion (LC) layer on polyethylene (PE) film using CD-polymers was directly generated, owing to the film-forming characteristics of polymers. Furthermore, a superhydrophobic coating, which is composed of polydimethylsiloxane (PDMS) and hydrophobic fumed silica, was constructed and connected with the LC layer via a PDMS intermediate layer. The transparent, UV-to-red light conversion and superhydrophobic self-cleaning multi-layers on PE (LCSHL-PE) were eventually produced. The water contact angle of the LCSHL-PE film is as high as 174° and the water rolling angle is less than 2°. In comparison to PE film, the LCSHL-PE can enhance red light irradiance by 9.44% while decreasing UV irradiance by 41.21%. More importantly, the obtained LCSHL-PE film displays outstanding mechanical robustness and weather durability, which would ensure its potential in agricultural applications.

Received 26th October 2023  
Accepted 17th December 2023

DOI: 10.1039/d3ta06551k

rsc.li/materials-a

## Introduction

Light conversion film (LCF), a type of functional film that allows for optical wavelength conversion, is crucial in improving solar energy utilization, particularly in the fields of photovoltaic power<sup>1</sup> and greenhouse agriculture.<sup>2,3</sup> For example, carotene, chlorophylls a and b as well as other photosynthetic pigments strongly absorb visible light in the blue (400–500 nm) and red (630–700 nm) regions. Among them, the largest photosynthetic quantum yield is provided by red light.<sup>4,5</sup> On the other hand, high-energy ultraviolet light (UV, 200–400 nm) not only inhibits photosynthesis but also makes plants more susceptible to diseases and infection.<sup>6</sup> Therefore, both UV-to-blue and UV-to-red conversion films have been highly desired to improve agricultural output and quality over the past decade.

However, in the process of outdoor use, the LCFs are inevitably polluted by dust, mud, snow and so on, significantly reducing their transmittance and operating life. Superhydrophobic

surfaces, governed by low surface energy and micro-nano roughness,<sup>7,8</sup> have been used in many applications, such as self-cleaning,<sup>9,10</sup> anti-fouling,<sup>11</sup> anti-corrosion,<sup>12,13</sup> and anti-icing.<sup>14,15</sup> Due to the high water contact angle (>150°) and low rolling angle (<10°) of superhydrophobic surfaces, surface pollutants or dust could naturally fall under the action of natural external forces like rain and wind. Thus, fabricating smart films with spectral conversion and superhydrophobic self-cleaning properties would be a feasible strategy for maintaining light transmittance and extending the service life of the LCFs.

As the crucial functional component of LCFs, light conversion agents (LCAs) primarily divide into three categories: inorganic compounds,<sup>16,17</sup> organic fluorescent dyes,<sup>18</sup> and organic rare earth complexes.<sup>19</sup> Generally, the existing LCAs still have various defects, such as poor matching between the LCA's emission and the absorption of plant pigments, low stability, poor dispersibility or exorbitant price. These flaws limit the application and further popularization of LCFs. Emerging as a new class of photoluminescent (PL) nanomaterials, carbon dots (CDs)<sup>20,21</sup> feature excellent optical properties (tunable emission and photostability), non-toxicity, and low-cost, which means they hold promise for applications in many fields such as photodynamic therapy,<sup>22</sup> bio-imaging,<sup>23</sup> sensing,<sup>24,25</sup> catalysis,<sup>26</sup> light-emitting diodes (LEDs)<sup>27,28</sup> and agricultural films.<sup>29</sup>

Functional Nanomaterials Laboratory, Centre for Micro/Nanomaterials and Technology, Key Laboratory of Photochemical Conversion and Optoelectronic Materials, Technical Institute of Physics and Chemistry, Chinese Academy of Sciences, Beijing 100190, China. E-mail: jhhe@mail.ipc.ac.cn

† Electronic supplementary information (ESI) available. See DOI: <https://doi.org/10.1039/d3ta06551k>



For example, Li *et al.* prepared dual-emissive CDs, whose blue and red emission perfectly match the absorption spectrum of chloroplasts, using *Phellodendron chinense* Schneid as carbon source, and applied them for enhancing biological photosynthetic efficiency.<sup>30</sup> Li and team prepared red-light emitting CDs (~680 nm, could be exactly absorbed by chlorophyll-a) with a quantum yield (QY) of 15.34% using spinach as precursor.<sup>31</sup> Despite such superior properties, all those reported CDs exhibit fluorescence in solution. In the aggregate state or solid-state, unfortunately, CDs usually exhibit fluorescence self-quenching because of excessive resonance energy transfer and direct  $\pi$ - $\pi$  interactions, which greatly restricts their application in LCFs.<sup>32</sup>

Among a few reported approaches to resist the aggregation-caused quenching (ACQ) of CDs, an effective method to achieve solid-state fluorescence (SSF) CDs would be to embed the CDs in a solid matrix of either polymers or inorganic substances,<sup>33-35</sup> where the solid matrix provides the CDs with space hindrance. For instance, He *et al.* synthesized organosilane-functionalized CDs with solid-state red-fluorescence using anhydrous citric acid, *N*-( $\beta$ -aminoethyl)- $\gamma$ -aminopropyl methyl dimethoxy silane (KH-602) and acetone as reactants.<sup>36</sup> The quantum yield of the CDs sharply decreases, however, from 50.7% in aqueous solution to 9.60% in solid state. They further dispersed the red-emission CDs in solid matrixes (starch,  $\text{RnOCH}_2\text{COONa}$ , and  $\text{Al}_2\text{O}_3$ ), and obtained dual-fluorescence powders. Zhu *et al.* developed red SSF CDs through step-by-step post-modifications.<sup>37</sup> First, the modulation of CD aqueous solution with CTAB resulted in an increase of QY from 23.2% to 43.6%. They then dispersed the CTAB-modified CDs in a PVP matrix and obtained an SSF-CD film with a QY of 41.3%. The preparation of SSF CDs is frequently accompanied by a reduction in FL intensity and complicated post-modifications. Thus, a novel, simple strategy is required for manufacturing high FL quantum yield SSF CDs towards LCF applications.

Herein, we successfully synthesized, in a one-pot manner, a series of red-light emitting SSF CDs (named as CD-PVP and CD-PEG) using spinach as carbon source and polyvinyl pyrrolidone (PVP-K30) or polyethylene glycol (PEG-1000) as wrapping agent. The resulting CD-PVP and CD-PEG are easy to form solid-state luminescent films of high transparency on substrates, due to the CD dispersing effect and film-forming ability of PEG and PVP. We further designed and fabricated novel robust, durable and transparent tri-layer films with precise UV-to-red spectral conversion and excellent self-cleaning properties by first coating the obtained CD-PVP (or CD-PEG) on commercially available polyethylene (PE) film, then dip-coating a polydimethylsiloxane (PDMS) layer, followed by spray-coating a PDMS/hydrophobic fumed silica (HF-SiO<sub>2</sub>) layer. To our best knowledge, the light conversion and superhydrophobic multi-layer on PE film (LCSHL-PE) has not yet reported and would have tremendous potential for outdoor agricultural applications.

## Experimental

### Materials

Spinach was purchased from local supermarkets. Polyethylene glycol 1000 (PEG 1000) and polyvinylpyrrolidone K30 (PVP K30, molecular weight 40 000) were obtained from Shanghai Yuanye

Bio-Technology Co. (China). Hydrophobic fumed silica (AEROSIL R972, ~16 nm) was purchased from Evonik Degussa Co. (Germany). Polydimethylsiloxane (PDMS) prepolymer (Sylgard 184, including polymer and curing agent) was obtained from Dow Corning Co. (USA). Ethanol was offered by Modern Oriental (Beijing) Technology Development Co. (China). Hexane (GC,  $\geq 99\%$ ) was supplied by Shanghai Aladdin Biochemical Technology Co. (China). Linear low density polyethylene (LLDPE) films (100  $\mu\text{m}$ ) were purchased from Baishan Xifeng plastic Co.

### Synthesis of CDs using spinach as carbon resource (S-CDs)

The S-CDs were synthesized according to a reported method with some modifications.<sup>30</sup> Fresh spinach leaves (15 g) were grounded in 40 mL ethanol, then the obtained extraction was transferred into a 100 mL Teflon-lined autoclave, followed by heating at 150 °C for 7 h. The resultant mixture was filtered by 0.22  $\mu\text{m}$  organic-system syringe filter. Finally, the filtrate was freeze-dried to obtain solid S-CDs.

### Synthesis of polymer wrapped CDs

Fresh spinach leaves (10 g) were firstly ground by pestle and mortar, then extracted with ethanol (30 mL) for 30 min. The obtained clear spinach extraction was mixed with an ethanol solution (10 mL) of PVP K30 (0.5 g), then transferred into a 100 mL Teflon-lined autoclave, followed by heating at 150 °C for 7 h. The resultant mixture was filtered by 0.22  $\mu\text{m}$  organic-system syringe filter. Finally, a CD-PVP<sub>0.5</sub> solution was obtained and stored at 4 °C for subsequent operation. Furthermore, instead of 0.5 g, other amounts (0, 0.2, and 1 g) of PVP K30 were also used in the synthetic system, and the corresponding samples were referred to as S-CD, CD-PVP<sub>0.2</sub>, and CD-PVP<sub>1</sub>.

The PEG 1000 modified CDs were synthesized similarly to the synthetic strategy of PVP K30 modified CDs, except that varied amounts (0.5, 1, and 2 g) of PEG 1000 were added into the system. The obtained products were named as CD-PEG<sub>0.5</sub>, CD-PEG<sub>1</sub>, and CD-PEG<sub>2</sub>.

### Preparation of LCSHL-PE films

First, a PE film was cleaned with deionized water and ethanol for 10 min, respectively, followed by oxygen plasma cleaning for 5 min. Then the cleaned PE film was immersed in the CD-PVP<sub>0.5</sub> (or CD-PEG<sub>1</sub>) solution for varied times (3, 6, 9, 12, 15) of dip-coating (immersion time: 60 s, withdrawing speed: 100  $\text{mm min}^{-1}$ ). After each dip-coating, the film was dried at 40 °C for 5 min. Next, a *ca.* 40% PDMS solution (6 g PDMS and 0.6 g curing agent were dissolved in 10 g hexane) was dip-coated twice on the above film, followed by drying at 60 °C for 15 min, and a partially cured PDMS interlayer was obtained. Then a pre-prepared suspension of PDMS, hydrophobic fumed silica, and hexane (mass ratio: 10 : 3 : 100) was immediately spray-coated onto the partially cured PDMS interlayer, where the distance between the spray gun and the film was kept at 10–15 cm and the spray pressure was 0.3–0.5 MPa. Finally, the sample was cured at 60 °C for another 2 h, giving light conversion and superhydrophobic self-cleaning tri-layer coatings.



### Durability and mechanical stability tests of superhydrophobic surfaces

To verify the durability and mechanical stability of superhydrophobic surfaces, several tests were carried out. Specifically, the tape peeling test was carried out by pressing a 3 M tape on with 1 kg weight and peeling off the surface 0, 20, 40, 70, and 100 times, respectively. For the bending test, the LCSHL-PE film was subjected to bending experiments 2000 times. For the water drop impact test, 200 mL water (~6000 water droplets) was dropped to the surface from a height of 50 cm with a fall speed of  $1 \text{ m s}^{-1}$ , and the test was repeated 10 times.

### Environmental adaptability tests of LCSHL-PE film

The anti-attenuation of fluorescence and environmental adaptability are critical parameters to evaluate the practical application of the LCSHL-PE film, for which water immersion tests, temperature and humidity tests, and sunlight exposure tests were conducted, respectively. To simulate the stability of the LCSHL-PE film in rainy weather, we soaked it in tap water and measured its fluorescence emission and WCA at intervals. For the temperature and humidity tests, the LCSHL-PE film was placed in a chamber of constant temperature ( $40 \text{ }^\circ\text{C}$ ) and humidity (80% RH). The LCSHL-PE film was directly exposed to sunlight for its light stability tests. The fluorescent emission and WCA were measured at regular intervals within 21 d. To investigate the UV stability of the films, we placed the PE, LC-PE, and LCSHL-PE films under a 365 nm UV lamp (8 W, with a distance of 10 cm between the films and the lamp) for 72 h of continuous irradiation.

## Results and discussion

The CDs wrapped with polymers (CD-PVP, and CD-PEG) were prepared by one-pot solvothermal treatment of spinach extract and different amounts of PVP K30 (or PEG 1000), as illustrated in Fig. 1a. All the obtained CD-polymer (modified with different amounts of PVP and PEG) solutions exhibit the same fluorescence properties as the original S-CDs solution, the maximum excitation and emission centering at 410 nm and 673 nm, respectively (Fig. S1 and S2†). The fluorescence emission of these CDs perfectly matches the absorption of chlorophyll a in the red-light region, thereby having great potential to effectively enhance plant photosynthesis. Moreover, it is worth noting that CD-PVP and CD-PEG possess higher fluorescence quantum yield than the S-CD (15.80%, under the excitation at 410 nm), especially CD-PVP<sub>0.5</sub> with a QY of 16.70% and CD-PEG<sub>1</sub> with a QY of 16.85% (Table S1†).

To elucidate the mechanism of the high QY of the CD-polymers, the chemical composition and surface structure of S-CD, CD-PVP<sub>0.5</sub>, and CD-PEG<sub>1</sub> were investigated by XPS and FTIR. The XPS survey spectra indicate that the S-CD, CD-PVP<sub>0.5</sub>, and CD-PEG<sub>1</sub> are all composed of C, O, and N (Fig. 1b). Specifically, the high-resolution C 1s spectra of all CDs demonstrate the existence of C-C/C=C, C-N, C-O, and C=O/C=N in all these CDs (Fig. 1d). The N 1s spectra of all CDs reveal four peaks that correspond to pyridine N (C-N=C), pyrrole N

(C-N-C), graphitic N (N-(C)<sub>3</sub>), and amino N (Fig. 1e). The O 1s spectra of all CDs contain three peaks that are assigned to C=O, C-OH/C-O-C, and C-O (Fig. 1f). These results prove that the surfaces of all CDs are rich in polyaromatic, carboxyl, and amino structures. Additionally, as shown in Fig. 1c, the surface O and N atomic concentrations in CD-PVP<sub>0.5</sub> are 17.43% and 3.56%, and in CD-PEG<sub>1</sub> are 24.03% and 3.46%, respectively, which are higher than those in S-CD (O 16.00% and N 3.15%). Moreover, the high-resolution spectra of N 1s, O 1s, and C 1s show an apparent discrepancy in the proportion of different fine structures in S-CD and CD-PVP<sub>0.5</sub>. For instance, CD-PVP<sub>0.5</sub> has higher proportions of pyrrole N and C=O bonds than S-CD, demonstrating that PVP had been wrapped around the surface of CD (Fig. 1i). Similarly, the increased fraction of C-O bonds in CD-PEG<sub>1</sub> investigated the distribution of PEG chains on the surface of CD-PEG<sub>1</sub> (Fig. 1h).

What's more, in the FTIR spectrum of CD-PVP<sub>0.5</sub> (Fig. 2a), the peaks of C-N stretching at  $1290 \text{ cm}^{-1}$  and C=O stretching at  $1651 \text{ cm}^{-1}$  of PVP, and the peaks of N-H stretching of the porphyrin ring at  $3282 \text{ cm}^{-1}$  and O-C=O stretching at  $1454 \text{ cm}^{-1}$  of S-CD shift to  $1288 \text{ cm}^{-1}$ ,  $1664 \text{ cm}^{-1}$ ,  $3286 \text{ cm}^{-1}$  and  $1460 \text{ cm}^{-1}$ , respectively, which are attributed to the hydrogen bond interaction. These observations indicate that PVP is wrapped on the surface of CD by hydrogen bonding. Meanwhile, the broad peak of CD-PEG<sub>1</sub> in the range of  $3100 \text{ cm}^{-1}$  to  $3600 \text{ cm}^{-1}$ , attributed to the vibration of -OH and -COOH, is weaker than that in S-CD (Fig. 2b). Compared with the PEG, a new band of O-C=O stretching at  $1450 \text{ cm}^{-1}$  appears in CD-PEG<sub>1</sub>. In addition, the peak of O-C=O stretching in CD-PEG<sub>1</sub> is stronger than that in S-CD. These results indicate that PEG is wrapped on the surface of CD by the condensation reaction between the -OH groups in PEG and -COOH groups in S-CD. It is speculated from the above data that the improvement of QYs of CD-PVP and CD-PEG are due to the polymer spacers that effectively prevent the fluorescence quenching caused by CDs aggregation.<sup>38,39</sup>

The optical properties of CD-PVP<sub>0.5</sub> and CD-PEG<sub>1</sub> in both solution and solid state were further investigated to verify the effects of polymer spacers in protecting CDs from ACQ. The UV-Vis absorption spectra in Fig. 2c and d display that all the polymers modified CDs solutions and solids possess the same typical absorption peaks as S-CD, including the peaks at 271 nm ( $\pi$ - $\pi^*$  transition of aromatic rings), 414 nm (soret band, a<sub>1u</sub> ( $\pi$ )-eg ( $\pi^*$ ) transition of porphyrins), and 500–700 nm (Q-band of porphyrins). The PL excitation and emission spectra of all the polymers modified CDs solutions exhibit an excitation peak located at 410 nm and an emission peak located at 673 nm, which have no noticeable change compared with the PL spectra of S-CD solution (Fig. 2c-f). However, both the excitation (416 nm) and emission peaks (677 nm) of the solid polymers modified CDs present a slight red-shift, that might be related to their close proximity to each other in the solid state. And the CIE 1931 chromaticity diagrams of CD solutions and solid CDs are shown in Fig. 2g and h. Furthermore, under the excitation of a 365 nm UV lamp the solid CD-PVP<sub>0.5</sub> and CD-PEG<sub>1</sub> show bright red emission, whereas the solid S-CD shows no emission (Fig. S3†). More excitingly, the QYs of solid-state CD-PVP<sub>0.5</sub> and CD-PEG<sub>1</sub>



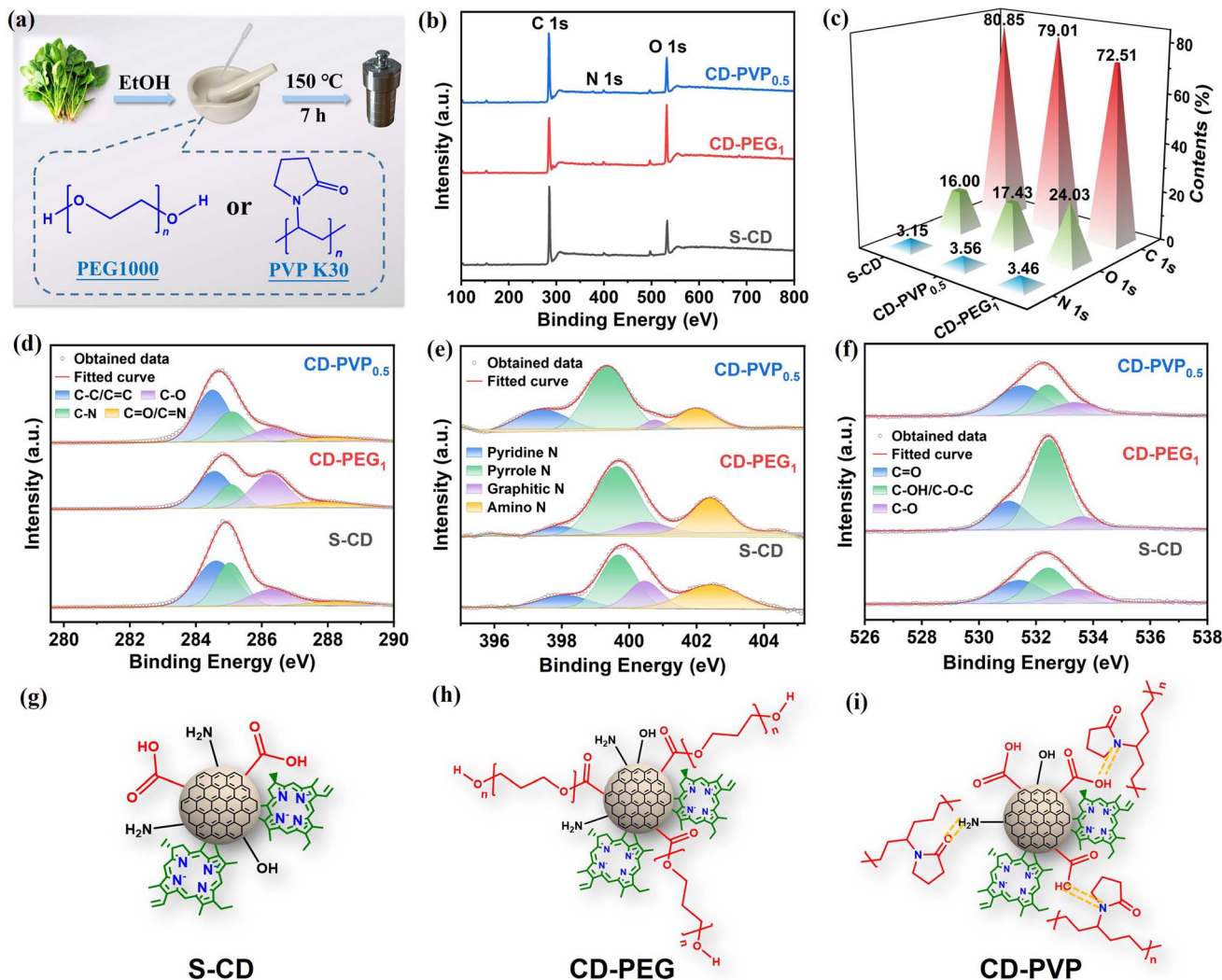


Fig. 1 (a) Schematic diagram for preparation of polymer-wrapped CDs. (b) XPS survey spectra of S-CD, CD-PVP<sub>0.5</sub>, and CD-PEG<sub>1</sub>. (c) Ratios of C 1s, O 1s, and N 1s in S-CD, CD-PVP<sub>0.5</sub>, and CD-PEG<sub>1</sub>. (d) High-resolution C 1s spectra of S-CD, CD-PVP<sub>0.5</sub>, and CD-PEG<sub>1</sub>. (e) High-resolution N 1s spectra of S-CD, CD-PVP<sub>0.5</sub>, and CD-PEG<sub>1</sub>. (f) High-resolution O 1s spectra of S-CD, CD-PVP<sub>0.5</sub>, and CD-PEG<sub>1</sub>. The structure schematic diagram of S-CD (g), CD-PEG (h), and CD-PVP (i).

reach 19.53% and 20.91%, respectively, which are higher than those in the solution-state (Table S2<sup>†</sup>). These results indicate that the introduction of polymers spacers between CDs by wrapping them effectively conquers the ACQ phenomenon.

Moreover, TEM observations (Fig. 3a–c) display that the average diameters of CD-PVP<sub>0.5</sub> and CD-PEG<sub>1</sub> are  $6.19 \pm 0.40$  nm and  $6.06 \pm 0.30$  nm, respectively, which are larger than that of S-CD ( $4.70 \pm 0.25$  nm). Combined with the above data, the increase in size ( $\sim 1.40$  nm) of CD-polymers more intuitively expresses the wrapping of polymers on the surface of CDs.

Furthermore, the FL lifetimes and dynamics of the polymers wrapped CDs in solution and solid state were investigated to clarify the aggregation-quenching resistant mechanism of solid CD-PVP and CD-PEG. By fitting the fluorescence decay curves (Fig. 3d and e), the CD-PVP<sub>0.5</sub> ethanol solution and solid CD-PVP<sub>0.5</sub> show single exponential lifetimes ( $\tau$ ) of 7.08 ns and 8.19 ns, while those of CD-PEG<sub>1</sub> in solution and solid state are 7.18

ns and 8.75 ns, respectively. Next, the rate constants of radiative ( $k_r$ ) and nonradiative ( $k_{nr}$ ) decays of CD-polymers in solution and solid state were calculated from the QY and lifetimes ( $\tau$ ) using the equations:

$$\frac{k_r}{k_r + k_{nr}} = \text{QY} \quad (1)$$

$$k_r + k_{nr} = \frac{1}{\tau} \quad (2)$$

As shown in Table S2<sup>†</sup>, the  $k_r$  and  $k_{nr}$  of solid CD-polymers ( $k_r = 2.38 \times 10^7 \text{ s}^{-1}$  and  $k_{nr} = 9.83 \times 10^7 \text{ s}^{-1}$  for CD-PVP<sub>0.5</sub>,  $k_r = 2.39 \times 10^7 \text{ s}^{-1}$  and  $k_{nr} = 9.04 \times 10^7 \text{ s}^{-1}$  for CD-PEG<sub>1</sub>) are approximate to those of solution ( $k_r = 2.36 \times 10^7 \text{ s}^{-1}$  and  $k_{nr} = 11.76 \times 10^7 \text{ s}^{-1}$  for CD-PVP<sub>0.5</sub>,  $k_r = 2.35 \times 10^7 \text{ s}^{-1}$  and  $k_{nr} = 11.58 \times 10^7 \text{ s}^{-1}$  for CD-PEG<sub>1</sub>). These results demonstrate that the solid CD-polymers maintain similar excited state characters



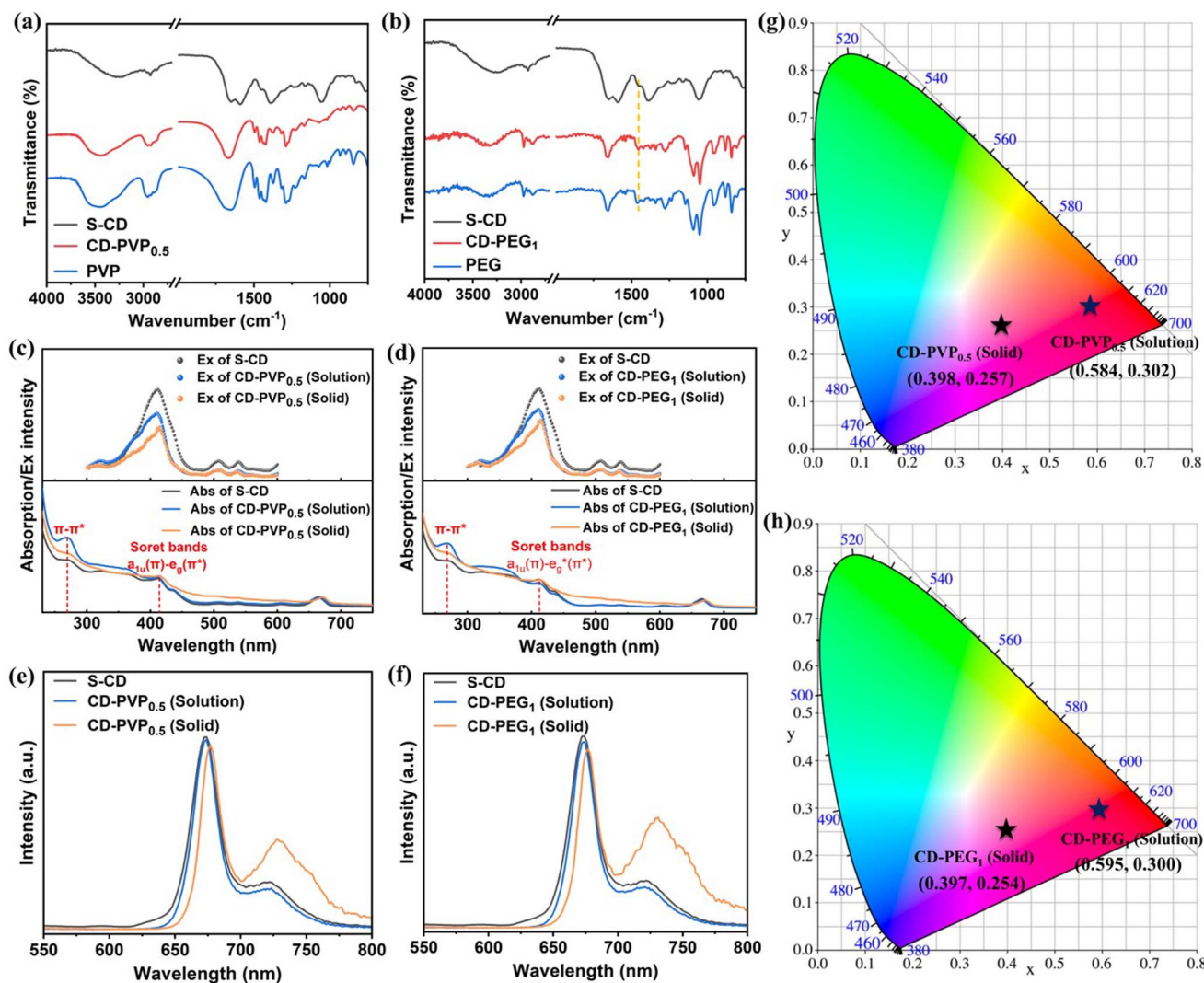


Fig. 2 (a) FTIR spectra of S-CD, CD-PVP<sub>0.5</sub>, and PVP. (b) FTIR spectra of S-CD, CD-PEG<sub>1</sub>, and PEG. UV-Vis absorption (down) and PL excitation (up) spectra of (c) original S-CD ethanol solution, CD-PVP<sub>0.5</sub> ethanol solution, and solid CD-PVP<sub>0.5</sub>, (d) and S-CD solution, CD-PEG<sub>1</sub> solution, and solid CD-PEG<sub>1</sub>. PL emission spectra of (e) original S-CD ethanol solution, CD-PVP<sub>0.5</sub> ethanol solution, and solid CD-PVP<sub>0.5</sub>, (f) S-CD solution, CD-PEG<sub>1</sub> solution, and solid CD-PEG<sub>1</sub> under 410 nm excitation. CIE 1931 color coordinates of (g) CD-PVP<sub>0.5</sub> solution and solid CD-PVP<sub>0.5</sub>, (h) CD-PEG<sub>1</sub> solution and solid CD-PEG<sub>1</sub>.

as in solution because of the wrapping of polymers on the CD surface. In addition, the slightly longer lifetimes and decreased  $k_{nr}$  of solid CD-polymers might be caused by the reduction of nonradiative transition and energy loss arising from the interaction of CDs and ethanol.<sup>40</sup> On the other hand, the resonance energy transfer (RET) and direct  $\pi$ - $\pi$  interaction between CDs in the aggregate state could be effectively avoided due to the spacing and steric hindrance provided by the polymers (Fig. 3f).

In addition to preventing the ACQ of CDs, the wrapping by PVP and PEG also endow CDs with favorable film-forming properties. Compared with S-CD, both CD-PVP<sub>0.5</sub> and CD-PEG<sub>1</sub> could form a uniform and fluorescent coating on PE substrate by dip-coating. Here, we directly dipped pretreated PE substrates in the as-synthesized CD-polymer ethanol solutions several times (including 3, 6, 9, 12, and 15 times), and obtained light conversion composite PE films (LC-PE). These prepared

LC-PE films would, however, not be stable enough for practical applications because of the hydrophilicity of PEG and PVP. Considering these issues, we further designed and constructed the d tri-layer films by adding an adhering PDMS interlayer and a superhydrophobic outer layer composed of PDMS and hydrophobic fumed silica on the light conversion layer (Fig. 4a).

From cross-sectional SEM observations (Fig. 4b), it could be found that the obtained light conversion and superhydrophobic tri-layer films are firmly adhered to both sides of PE film (LCSHL-PE). And the thickness of the tri-layer films is *ca.* 25  $\mu$ m. As shown in Fig. 4c, the SEM image displays the rough surface of the LCSHL-PE film. The hierarchical surface structure is composed of nano, submicron, and micron structures, that exist alone as itself or are formed by the aggregation of hydrophobic fumed silica nanoparticles. In addition, the silicon nanoparticles are encapsulated by the PDMS layer. Therefore,



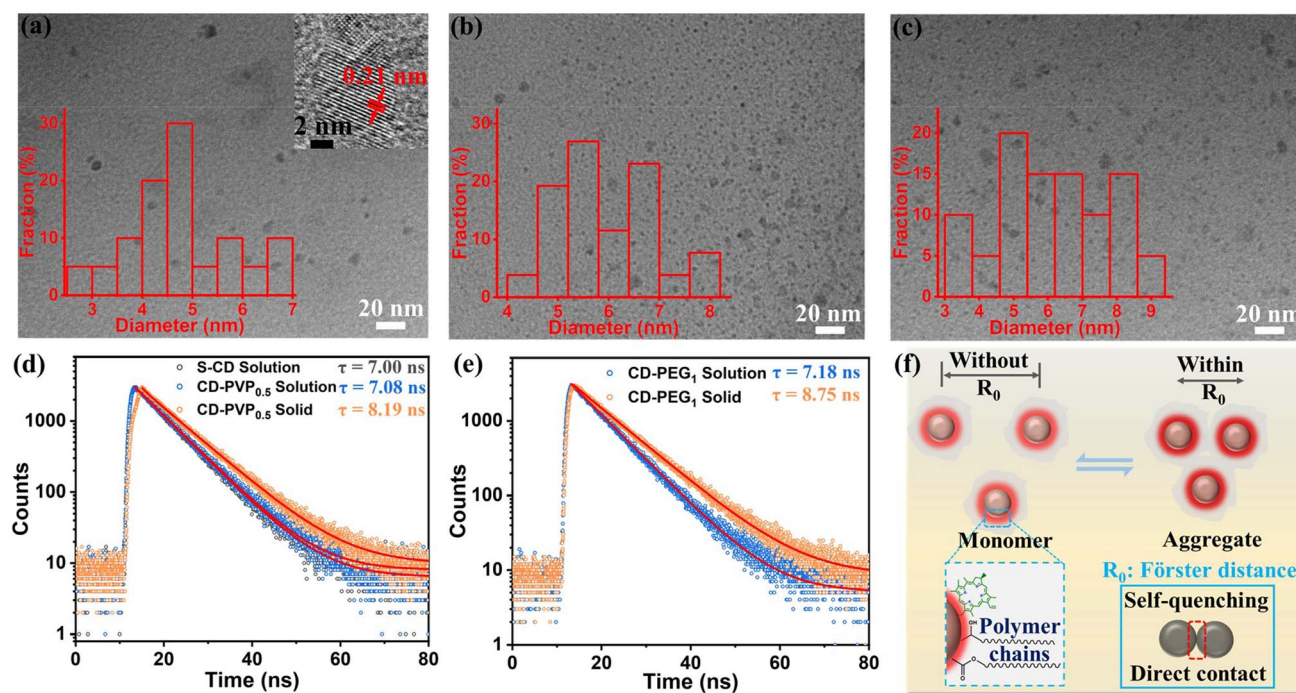


Fig. 3 TEM images of (a) S-CD, (b) CD-PVP<sub>0.5</sub>, and (c) CD-PEG<sub>1</sub>, insets are HRTEM image and size distribution histograms. Fluorescence decay curves collected at 670 nm under 405 nm excitation of (d) S-CD solution, CD-PVP<sub>0.5</sub> solution, and solid CD-PVP<sub>0.5</sub> and (e) CD-PEG<sub>1</sub> in both solution and solid state. (f) Schematic mechanism of aggregation quenching resistance of solid polymer wrapped CDs.

the micro/nano rough surface combines with the low surface energy of PDMS to present the super-hydrophobicity of LCSHL-PE. The water, milk, and orange juice droplets randomly distributed on the surface are nearly spherical (Fig. 4d), which verifies the superhydrophobicity of LCSHL-PE.

We also investigated the wettability of the surface by measuring its water contact angle (WCA) and rolling angle (RA). Compared with the original PE film (WCA: 71°, Fig. S4b†) and smooth PDMS surface (WCA: 122°, Fig. S4d†), the WCA of the composite film is significantly improved. From Fig. 4e and f, we could find that the LCSHL-PE surface possesses a WCA of up to 174° and a RA of about 2°. Moreover, based on the high WCA and low RA, the LCSHL-PE film exhibits satisfactory self-cleaning performance. As shown in Fig. 4g, the water droplet (5 μL) was pushed against the LCSHL-PE surface, demonstrating the excellent non-adhesion and self-cleaning properties. Furthermore, the superhydrophobicity of the LCSHL-PE film was also indicated by the 3 bounces of an 8 μL water droplet on the surface (Fig. S5 and Movie S1†). As shown in Fig. 4h and Movie S2,† methylene blue-stained water droplets could easily carry away sand particles on the LCSHL-PE, which was placed at *ca.* 6° relative to the horizontal plane. What's more, the LCSHL-PE film could still maintain its self-cleaning performance when exposed to oil (hexane, Fig. 4i and Movie S3†).

Furthermore, it is noted that both the LC-PE, which only dip-coated the CD-polymers, and the LCSHL-PE with a superhydrophobic protective layer maintain transmittance comparable to that of blank PE in the visible region (Fig. 5a, S6 and S7†). These observations are mainly because the as-synthesized

CD-polymers absorb ultraviolet with wavelength below 420 nm, and has almost no effect on the transmission of visible light. According to the Mie scattering theory, when the size of surface particle is close to or greater than the wavelength of incident light, the scattering cross-section ( $\sigma_s$ ) is proportional to the square of the particle diameter ( $d$ ), as shown in the eqn (3):<sup>41–43</sup>

$$\delta_s = \frac{\pi d^2}{2} \sum_{n=1}^{\infty} (2n+1)(a_n + b_n) \quad (3)$$

where  $d$  is the diameter of the particles,  $a_n$  and  $b_n$  are the Mie coefficients of order  $n$  and related to the electromagnetic properties of the material.

Therefore, the uniform distribution of silica nanoparticles on the surface, without increase in light scattering caused by large particle aggregation, is another important factor for the high transmittance of LCSHL-PE. Overall, the rough surface of LCSHL-PE film in this work not only provides conditions for superhydrophobicity, but also maintains transparency, which is crucial for light conversion agricultural films.

The fluorescence emission spectra and spectral irradiance were measured to investigate the light conversion property of the LCSHL-PE films. As shown in Fig. 5b, S8 and S9,† both the LC-PE and LCSHL-PE films have emission spectra with a peak of 677 nm under excitation at 410 nm. And the inset photos exhibit that all the prepared films (LC-PE and LCSHL-PE) emit bright red fluorescence under the irradiation of a 365 nm ultraviolet lamp. In addition, the FL intensity of LC-PE films, coated with different numbers of CD-polymers layers (3, 6, 9, 12, and 15 layers), enhances with increasing the number of coating layers.



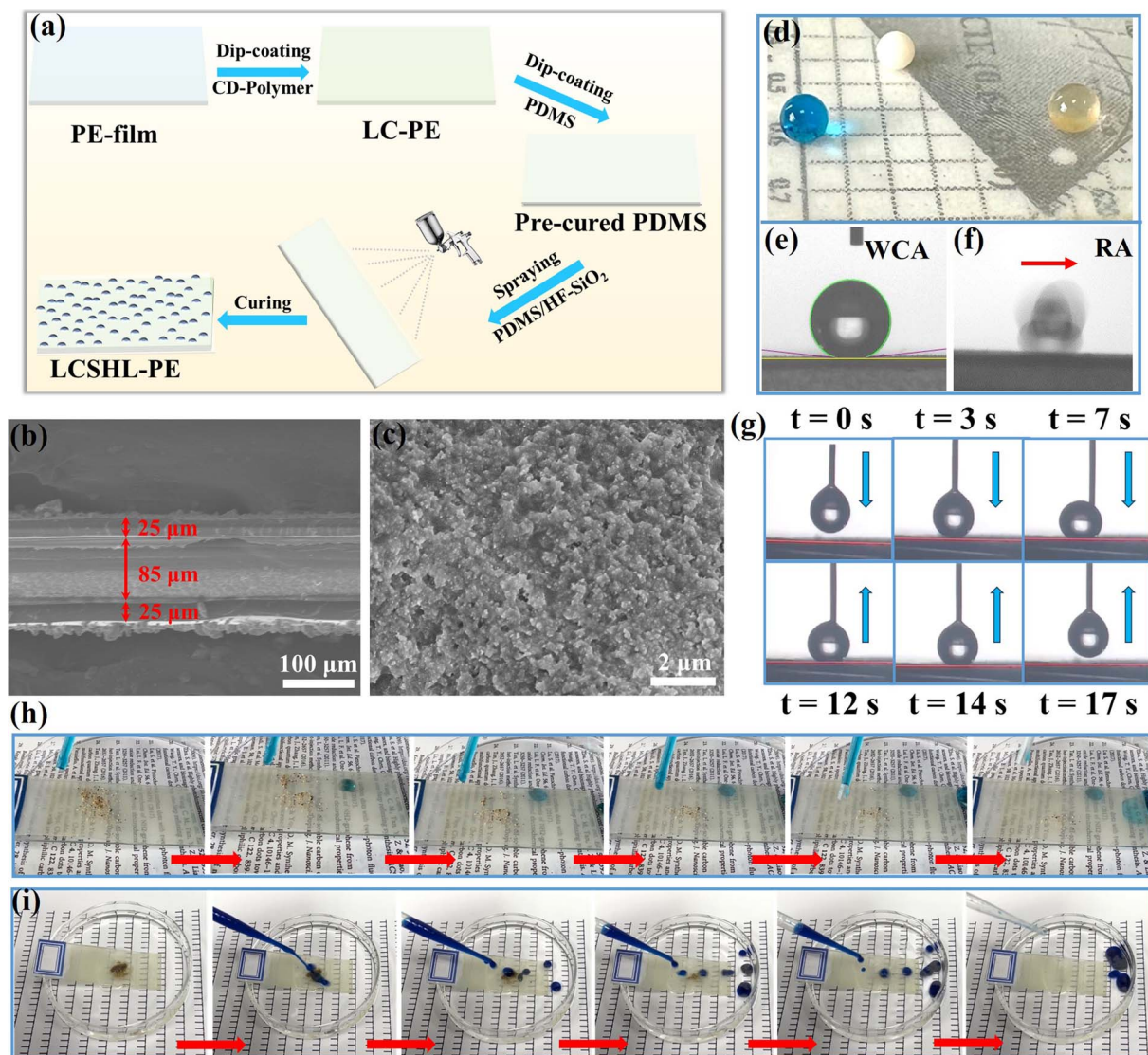


Fig. 4 (a) Illustration of the preparation process of LCSHL-PE film. (b) SEM image of the cross-section of LCSHL-PE film. (c) SEM image of the surface of LCSHL-PE film. (d) Photograph of water (blue, dyed with methylene blue), milk (white), and orange juice (yellow) droplets on the surface of LCSHL-PE film. WCA (e) and WRA (f) of LCSHL-PE film. (g) Water droplet (5  $\mu\text{L}$ ) contacting and leaving the LCSHL-PE surface. (h) Photographs of self-cleaning test of the LCSHL-PE ((CD-PVP<sub>0.5</sub>)<sub>15</sub>). (i) Photographs of self-cleaning of LCSHL-PE exposed to hexane (the LCSHL-PE was fixed onto the glass plate using double-sided tape).

For the LCSHL-PE films with a superhydrophobic layer, their fluorescence maintains the same intensity as the C-PE films. Fig. 5c, S10 and S11<sup>†</sup> show the photosynthetic photon flux density (PPFD) of LC-PE and LCSHL-PE films under sunlight using a handheld plant lighting spectral detector (UPRtek PG-200N). In accordance with the FL spectra, the spectral irradiation intensity of both LCSHL-PE and LC-PE films enhances with increase of the number of CD-polymer layers, and the composite films with 15 layers of CD-polymer possess the optimal light conversion performance. The LCSHL-PE films absorb strongly in the ultraviolet region and emit in the red, leading to higher irradiance in red light than pure PE film. Remarkably, compared to pure PE film, the LCSHL-PE ((CD-PVP<sub>0.5</sub>)<sub>15</sub> and (CD-PEG<sub>1</sub>)<sub>15</sub>) films could shield 41.21% and 25.40% of UV (350–400 nm), respectively, while increasing PFD

in the red region by 9.44% and 3.35% (Fig. 5d and Table S3<sup>†</sup>). These results indicate that the fabricated LCSHL-PE film not only exhibits outstanding superhydrophobic self-cleaning properties while maintaining high transparency, but also displays favourable UV-to-red light conversion performance. Moreover, the self-cleaning, light transmittance, and light conversion performance of the composite films are unaffected by different types of PE substrates, such as LDPE, HDPE, LLDPE and so on (Fig. S12, Movies S4 and S5<sup>†</sup>).

The robustness of superhydrophobic surface is crucial in practical applications. Therefore, tape peeling test, bending test, and water drop impact test were conducted to study the mechanical robustness and durability of LCSHL-PE surfaces. Here, the LCSHL-PE ((CD-PVP<sub>0.5</sub>)<sub>15</sub>) film, with optimal superhydrophobicity and light conversion performance, was selected



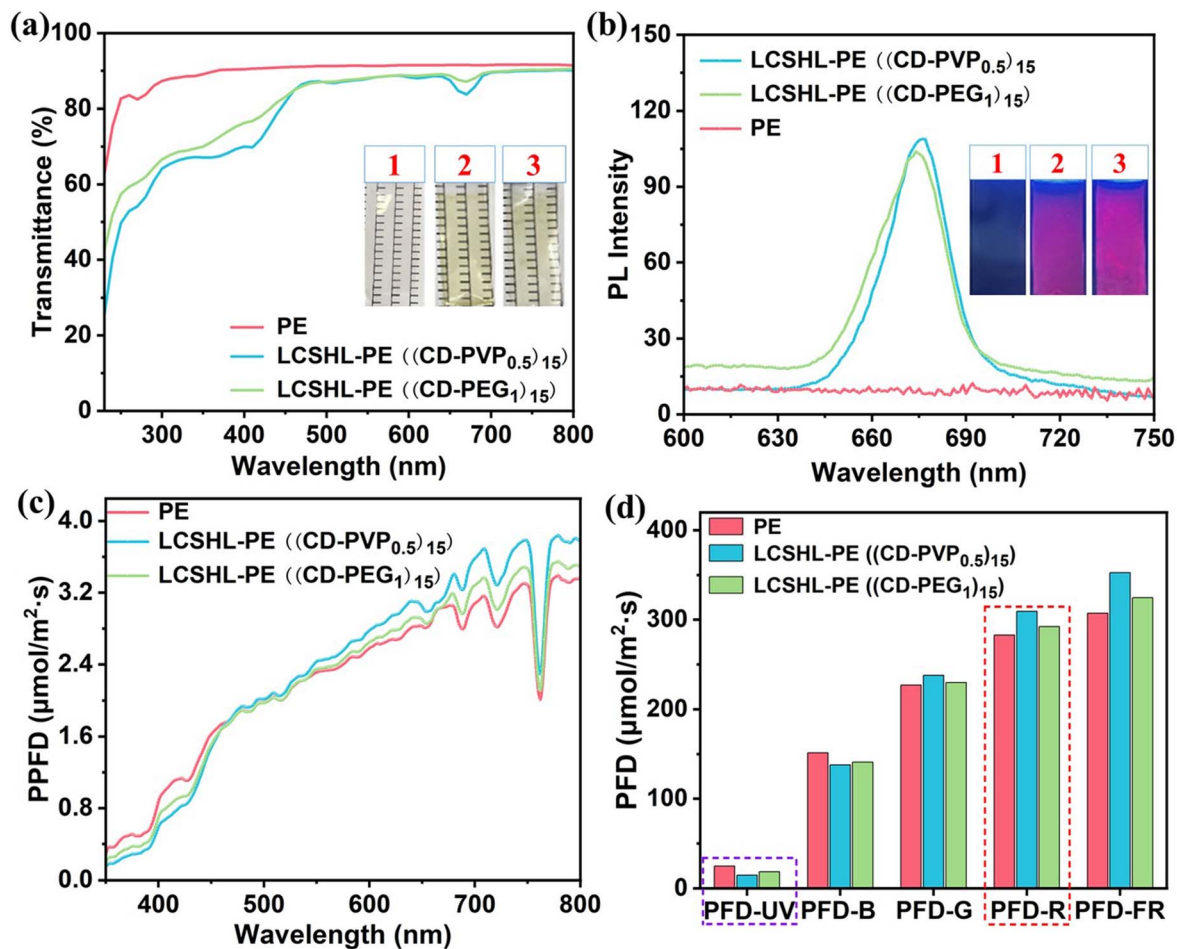


Fig. 5 (a) Transmittance and photographs (inset, under sunlight and placed on a printed paper with T) of PE, LCSHL-PE ((CD-PVP<sub>0.5</sub>)<sub>15</sub>), and LCSHL-PE ((CD-PEG<sub>1</sub>)<sub>15</sub>). (b) Fluorescent emission spectra and photographs (inset, under 365 nm UV lamp) of PE (1), LCSHL-PE ((CD-PVP<sub>0.5</sub>)<sub>15</sub>) (2) and LCSHL-PE ((CD-PEG<sub>1</sub>)<sub>15</sub>) (3). (c) PPFD of PE, LCSHL-PE ((CD-PVP<sub>0.5</sub>)<sub>15</sub>) and LCSHL-PE ((CD-PEG<sub>1</sub>)<sub>15</sub>). (d) PFD of blank PE, LCSHL-PE ((CD-PVP<sub>0.5</sub>)<sub>15</sub>) and LCSHL-PE ((CD-PEG<sub>1</sub>)<sub>15</sub>) in the UV, visible and infrared regions.

for the tests. 3 M tape was used to repeatedly stick on the LCSHL-PE surface with a 1 kg weight, followed by peeling it off the surface. After 100 repetitions, the WCA of the surface displayed a slight decrease ( $174^\circ$  to  $165^\circ$ ), and the WRA only increased from  $2^\circ$  to  $5^\circ$  (Fig. 6a), indicating that the hydrophobic fumed silica nanoparticles were firmly fixed by PDMS. It could be further confirmed from the SEM image and AFM image in Fig. 6b and c that the surface kept intact, still maintaining a regular micro/nano rough surface structure after the tape peeling test. In contrast, we found that when the mixture of hydrophobic fumed silica and *n*-hexane was sprayed on the pre-cured PDMS interlayer, the obtained surface showed a sharp decrease in WCA from  $172^\circ$  to  $148^\circ$  after the tape peeling test (Fig. S13<sup>†</sup>). SEM observations (Fig. S14<sup>†</sup>) reveal that the hydrophobic fumed silica loosely distributed on the surface was easily removed by the tape, resulting in serious damage to the superhydrophobicity of the surface. These results doubtlessly demonstrate that the anchoring of hydrophobic fumed silica by PDMS plays a crucial role in the robustness and durability of superhydrophobic surfaces.

Similarly, after 2000 cycles of bending test and 10 rounds of water impact test (each 200 mL of water dripping to the LCSHL-PE surface at a speed of  $1 \text{ m s}^{-1}$  from a height of 50 cm), the WCAs became  $169^\circ$  and  $168^\circ$ , respectively, remaining above  $160^\circ$ , while the WRAs were all below  $10^\circ$  (Fig. 6d and g). The SEM images and AFM images (Fig. 6e, f, h and i) show that the rough structure of the treated LCSHL-PE surfaces is still consistent with that before treatment, again indicating the good robustness and durability of the superhydrophobic surface.

The low attenuation rate of fluorescent emission of the LCSHL-PE film under natural conditions, including sun, moisture, and rain, is another significant indicator of its application performance. Therefore, water immersion test, temperature and humidity test, and sunlight exposure test were carried out to investigate the weather fastness of LCSHL-PE. As seen in Fig. 7a, following 240 h immersion in water, the FL emission intensity of the LCSHL-PE film exhibited an over 93% retention of the initial intensity, while its WCA only experienced minimal reduction. Additionally, our observations revealed that the hydrophobic layer maintained strong adhesion to the light conversion layer even after water immersion. In contrast, the FL



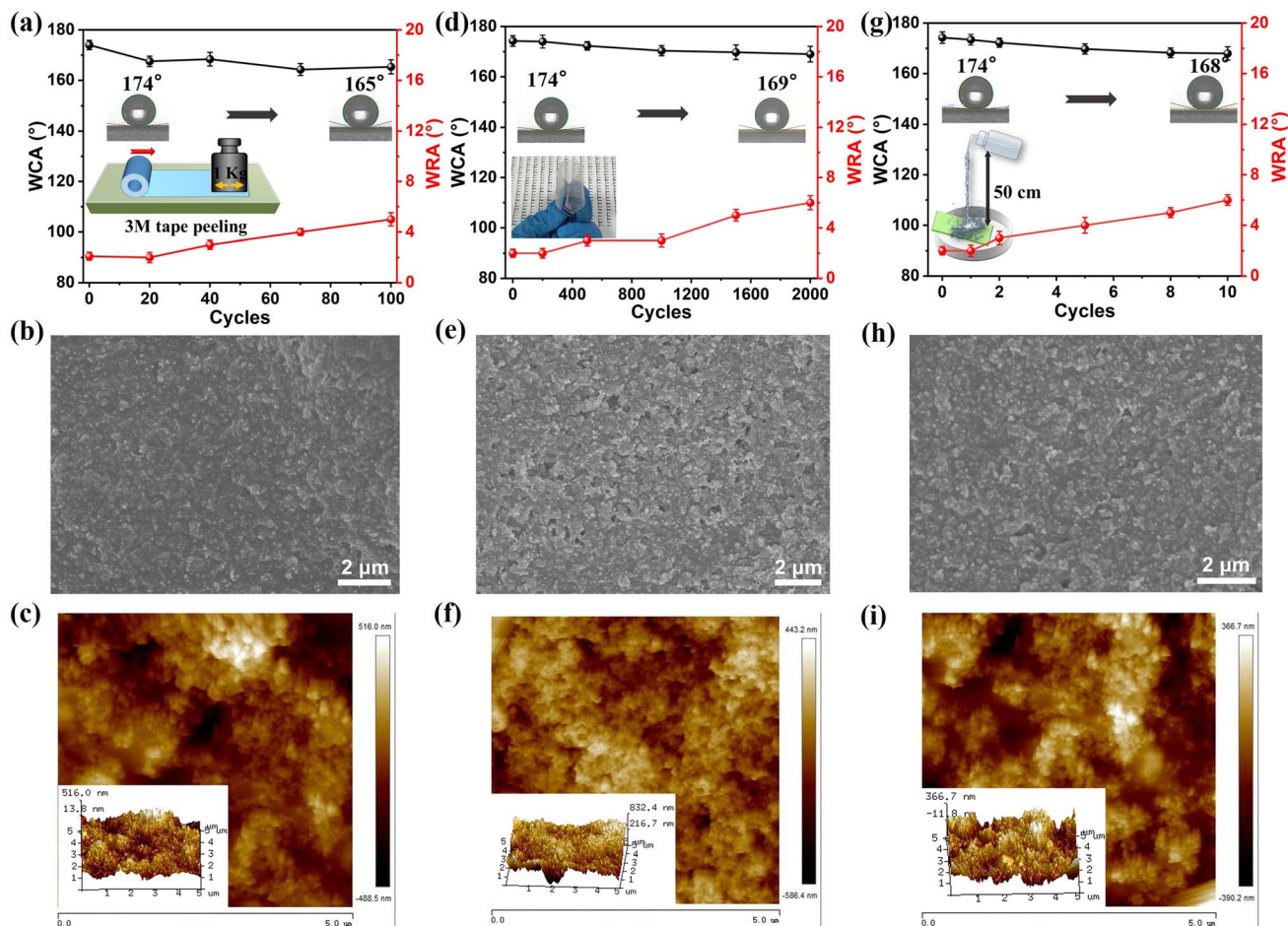


Fig. 6 WCAs and WRAs of LCSHL-PE film after multiple cycles of tape peeling test (a), bending test (d), and water drop impact test (g), insets: schematics of the tests, and images of water droplets on the film before and after the tests. SEM images of LCSHL-PE film surface after tape peeling test (b), bending test (e), and water drop impact test (h). 2D AFM images (insets: 3D AFM images) of LCSHL-PE film surface after tape peeling test (c), bending test (f), and water drop impact test (i).

intensity of the LC-PE film without a superhydrophobic layer exhibited a significant decline, maintaining only 56% of the original intensity (Fig. 7b and S15<sup>†</sup>). Similarly, after temperature and humidity (40 °C and 80% RH) treatment, the LCSHL-PE film demonstrates a more stable FL emission performance compared to the LC-PE film (Fig. 7c and d and S16<sup>†</sup>), as well as no significant alteration in WCA. These results suggest that the application of a superhydrophobic layer significantly enhances the water resistance and hydrothermal stability of LCSHL-PE films, while also demonstrating exceptional stability of the superhydrophobic layer.

The LCSHL-PE film also demonstrates consistent FL emission and superhydrophobicity under natural light. After 21 consecutive days of exposure, the FL intensity of both LCSHL-PE and LC-PE films remained above 85% of the original intensity (Fig. 7e and f and S17<sup>†</sup>), suggesting that the light conversion layer composed of CD-polymers exhibits exceptional light stability. Consequently, we could infer that the LCSHL-PE film possesses remarkable all-weather durability in terms of both superhydrophobicity and fluorescence emission. Moreover, as shown by SEM images in Fig. S18,<sup>†</sup> following 60 days of

exposure to natural light (similar to the practical application conditions), the structure of the LCSHL-film remained unchanged.

To investigate whether the CDs loading accelerates the UV aging of PE films as well as whether there are changes in the relative FL intensity and WCA, we exposed the PE, LC-PE and LCSHL-PE films to an 8 W 365 nm UV lamp for 72 h. As shown in Fig. 7g and S19,<sup>†</sup> the relative FL intensity of the LCSHL-PE film only minimally dropped, and it still maintained more than 92% of the initial FL intensity after UV treatment for 72 h. Furthermore, the WCA of the film also remained relatively stable following the UV treatment. Despite a relatively notable decline in FL intensity, the LC-PE still retained over 85% of its initial FL intensity (Fig. 7h), suggesting that the CDs have good UV stability. And the introduction of PDMS intermediate and superhydrophobic layer further enhanced the UV stability of the LC layer. Additionally, Fig. 7i and S20<sup>†</sup> show that the tensile strength and elongation at break of PE and LCSHL-PE films are nearly identical before and after UV treatment, indicating that the loading of CDs does not accelerate the UV aging of the PE films. Conversely, the CDs could be employed as a UV shielding



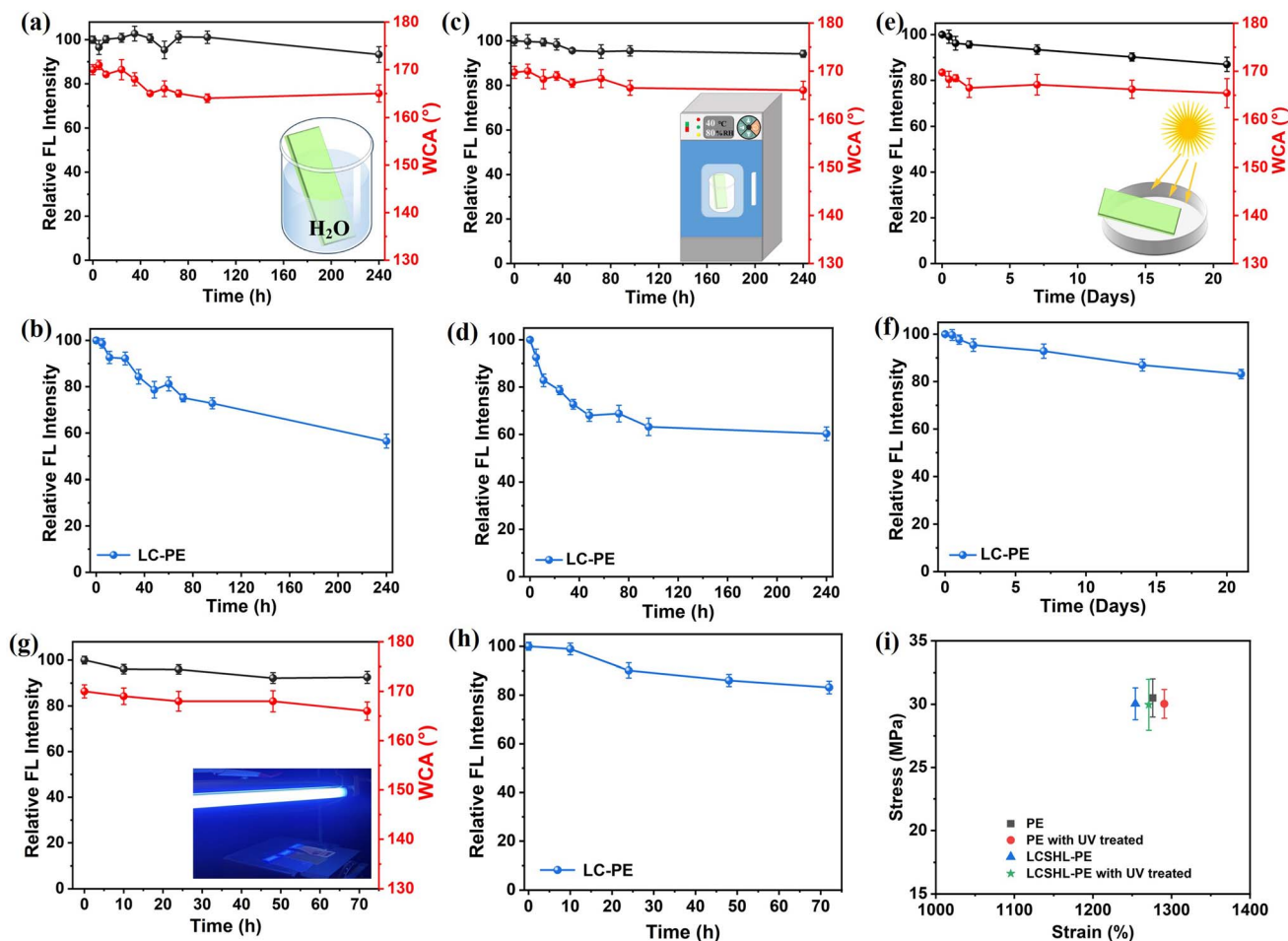


Fig. 7 Relative FL intensity and WCA of LCSSL-PE film after water immersion test (a), 40 °C temperature and 80% RH humidity test (c), sunlight exposure test (e), and UV treatment (g); insets: schematics of the tests. Relative FL intensity of LC-PE film after water immersion test (b), 40 °C temperature and 80%RH humidity test (d), sunlight exposure test (f), and UV treatment (h). (i) Stress–strain values of PE, LCSSL-PE and PE, LCSSL-PE after UV treated.

agent to increase the UV stability of PE films due to its capacity to absorb ultraviolet light and convert it into low-energy red-light.<sup>44,45</sup>

## Conclusion

In summary, we initially synthesized by a one-pot method a series of polymers-wrapped solid-state fluorescent CDs (CD-PVP and CD-PEG) with red emission precisely matching the plants photosynthesis need. The polymers wrapping imparts the CDs with the ability to mitigate the ACQ, as well as endows them with favorable film-forming properties. Then transparent UV-to-red light conversion layers were obtained by dip-coating the resulting CD-polymer onto PE film. Furthermore, a superhydrophobic layer was fabricated on the light conversion layer, which was composed of PDMS and hydrophobic fumed silica and anchored by a PDMS intermediate layer. Ultimately, a multilayer structure PE film comprising the light conversion and superhydrophobic layers (LCSSL-PE) was achieved, which exhibits exceptional transparency, superhydrophobic self-cleaning capability, and outstanding light conversion

performance. Moreover, the LCSSL-PE film demonstrates remarkable robustness in terms of its superhydrophobic self-cleaning property, while also showcasing all-weather durability in its light conversion performance. These findings highlight the immense potential of the LCSSL-PE film in agricultural production.

## Author contributions

Zhang S. and He J. designed the research approach together; Zhang S. performed the experiments and wrote the manuscript; He J. guided the research direction and revised the manuscript.

## Conflicts of interest

There are no conflicts to declare.

## Acknowledgements

This work was supported by the National Key Research and Development Program of China (2019QY(Y)0503,



2017YFA0207102), the National Natural Science Foundation of China (91963104, 52303286), Joint R&D Laboratory for Functional Agriculture Films, and Key Laboratory of Photochemical Conversion and Optoelectronic Materials. J. H. H. and S. N. Z. are grateful to CAS for a special postdoctoral support to S. N. Z.

## References

- 1 J.-S. Kang, J.-G. Kang, Y. Sohn and K. T. Leung, *ACS Appl. Mater. Interfaces*, 2018, **10**, 44768–44775.
- 2 J. He, Y. He, J. Zhuang, H. Zhang, B. Lei and Y. Liu, *Opt. Mater.*, 2016, **62**, 458–464.
- 3 T. G. Hwang, G.-Y. Kim, J.-I. Han, S. Kim and J. P. Kim, *ACS Sustainable Chem. Eng.*, 2020, **8**, 15888–15897.
- 4 S. Shoji, H. Saito, Y. Jitsuyama, K. Tomita, Q. Haoyang, Y. Sakurai, Y. Okazaki, K. Aikawa, Y. Konishi, K. Sasaki, K. Fushimi, Y. Kitagawa, T. Suzuki and Y. Hasegawa, *Sci. Rep.*, 2022, **12**, 17155.
- 5 L. Shen, R. Lou, Y. Park, Y. Guo, E. J. Stallknecht, Y. Xiao, D. Rieder, R. Yang, E. S. Runkle and X. Yin, *Nat. Food*, 2021, **2**, 434–441.
- 6 Y. Liu, Z. Gui and J. Liu, *Polymers*, 2022, **14**, 851.
- 7 S. G. Moghadam, H. Parsimehr and A. Ehsani, *Adv. Colloid Interface Sci.*, 2021, **290**, 102397.
- 8 X. Tian, T. Verho and R. H. A. Ras, *Science*, 2016, **352**, 142–143.
- 9 D. Wang, Q. Sun, M. J. Hokkanen, C. Zhang, F.-Y. Lin, Q. Liu, S.-P. Zhu, T. Zhou, Q. Chang, B. He, Q. Zhou, L. Chen, Z. Wang, R. H. A. Ras and X. Deng, *Nature*, 2020, **582**, 55–59.
- 10 C. Lu, Y. Gao, S. Yu, H. Zhou, X. Wang and L. Li, *ACS Appl. Mater. Interfaces*, 2022, **14**, 4750–4758.
- 11 F. Hizal, N. Rungraeng, J. Lee, S. Jun, H. J. Busscher, H. C. van der Mei and C.-H. Choi, *ACS Appl. Mater. Interfaces*, 2017, **9**, 12118–12129.
- 12 L. G. Greca, M. Rafiee, A. Karakoç, J. Lehtonen, B. D. Mattos, B. L. Tardy and O. J. Rojas, *ACS Nano*, 2020, **14**, 12929–12937.
- 13 F. Zhang, C. Zhang, L. Song, R. Zeng, S. Li and H. Cui, *J. Mater. Sci. Technol.*, 2015, **31**, 1139–1143.
- 14 W. Huang, J. Huang, Z. Guo and W. Liu, *Adv. Colloid Interface Sci.*, 2022, **304**, 102658.
- 15 Y. Wang, J. Xue, Q. Wang, Q. Chen and J. Ding, *ACS Appl. Mater. Interfaces*, 2013, **5**, 3370–3381.
- 16 D. Wang, H. Wang, B. Qian, H. Zou, K. Zheng, X. Zhou, Y. Song and Y. Sheng, *J. Lumin.*, 2020, **219**, 116844.
- 17 W. Wu, Z. Zhang, R. Dong, G. Xie, J. Zhou, K. Wu, H. Zhang, Q. Cai and B. Lei, *J. Rare Earths*, 2020, **38**, 539–545.
- 18 Y. Qi, Y. Wang, Y. Yu, Z. Liu, Y. Zhang, Y. Qi and C. Zhou, *J. Mater. Chem. C*, 2016, **4**, 11291–11297.
- 19 M. Zhang, C. Zhao, J.-Q. Song, W.-Q. He, P. Zhao and J. Liu, *Mater. Chem. Front.*, 2023, **7**, 160–167.
- 20 S. Li, L. Li, H. Tu, H. Zhang, D. S. Silvester, C. E. Banks, G. Zou, H. Hou and X. Ji, *Mater. Today*, 2021, **51**, 188–207.
- 21 B. Wang and S. Lu, *Matter*, 2022, **5**, 110–149.
- 22 A. Karagianni, N. G. Tsierkezos, M. Prato, M. Terrones and K. V. Kordatos, *Carbon*, 2023, **203**, 273–310.
- 23 J. Sobhanan, J. V. Rival, A. Anas, E. S. Shibu, Y. Takano and V. Biju, *Adv. Drug Delivery Rev.*, 2023, **197**, 114830.
- 24 N. Dhenadhayalan, K.-C. Lin and T. A. Saleh, *Small*, 2020, **16**, 1905767.
- 25 B. Li, T. Suo, S. Xie, A. Xia, Y.-J. Ma, H. Huang, X. Zhang and Q. Hu, *Trends Anal. Chem.*, 2021, **135**, 116163.
- 26 V. C. Hoang, K. Dave and V. G. Gomes, *Nano Energy*, 2019, **66**, 104093.
- 27 Y. Shi, W. Su, F. Yuan, T. Yuan, X. Song, Y. Han, S. Wei, Y. Zhang, Y. Li, X. Li and L. Fan, *Adv. Mater.*, 2023, 2210699.
- 28 L. Wang, W. Li, L. Yin, Y. Liu, H. Guo, J. Lai, Y. Han, G. Li, M. Li, J. Zhang, R. Vajtai, P. M. Ajayan and M. Wu, *Sci. Adv.*, 2020, **6**, eabb6772.
- 29 Y. Xie, X. Geng, J. Gao, W. Shi, Z. Zhou, H. Wang, D. Zhang, B. Deng and R. Yu, *J. Alloys Compd.*, 2021, **873**, 159663.
- 30 W. Li, S. Wu, H. Zhang, X. Zhang, J. Zhuang, C. Hu, Y. Liu, B. Lei, L. Ma and X. Wang, *Adv. Funct. Mater.*, 2018, **28**, 1804004.
- 31 L. Li, R. Zhang, C. Lu, J. Sun, L. Wang, B. Qu, T. Li, Y. Liu and S. Li, *J. Mater. Chem. B*, 2017, **5**, 7328–7334.
- 32 A. Xu, G. Wang, Y. Li, H. Dong, S. Yang, P. He and G. Ding, *Small*, 2020, **16**, 2004621.
- 33 C. Wang, T. Hu, Y. Chen, Y. Xu and Q. Song, *ACS Appl. Mater. Interfaces*, 2019, **11**, 22332–22338.
- 34 Y. Hao, Z. Gan, J. Xu, X. Wu and P. K. Chu, *Appl. Surf. Sci.*, 2014, **311**, 490–497.
- 35 F. Yan, H. Zhang, J. Xu, Y. Wu, Y. Zang and J. Sun, *ACS Sustainable Chem. Eng.*, 2021, **9**, 3901–3908.
- 36 J. He, Y. He, Y. Chen, B. Lei, J. Zhuang, Y. Xiao, Y. Liang, M. Zheng, H. Zhang and Y. Liu, *Small*, 2017, **13**, 1700075.
- 37 J. Zhu, X. Bai, X. Chen, Z. Xie, Y. Zhu, G. Pan, Y. Zhai, H. Zhang, B. Dong and H. Song, *Dalton Trans.*, 2018, **47**, 3811–3818.
- 38 Y. Qu, X. Bai, D. Li, X. Zhang, C. Liang, W. Zheng and S. Qu, *J. Colloid Interface Sci.*, 2022, **613**, 547–553.
- 39 H. Li, Z. Zhang, J. Ding, Y. Xu, G. Chen, J. Liu, L. Zhao, N. Huang, Z. He, Y. Li and L. Ding, *Carbon*, 2019, **149**, 342–349.
- 40 J. Guo, L. Qin and D. Wang, *J. Lumin.*, 2023, **257**, 119690.
- 41 P. Wang, M. Chen, H. Han, X. Fan, Q. Liu and J. Wang, *J. Mater. Chem. A*, 2016, **4**, 7869–7874.
- 42 S. G. Lee, D. S. Ham, D. Y. Lee, H. Bong and K. T. Cho, *Langmuir*, 2013, **29**, 15051–15057.
- 43 K. L. Cho, I. I. Liaw, A. H. F. Wu and R. N. Lamb, *J. Phys. Chem. C*, 2010, **114**, 11228–11233.
- 44 J. Qiu, W. Ye, C. Chen, Z. Xu, C. Hu, J. Zhuang, H. Dong, B. Lei, G. Hu and Y. Liu, *J. Ind. Eng. Chem.*, 2023, **117**, 442–449.
- 45 L. Wang, X. Liu, P. Qi, J. Sun, S. Jiang, H. Li, X. Gu and S. Zhang, *Carbohydr. Polym.*, 2022, **278**, 118957.

